Anomalous Behavior of 2D Janus Excitonic Layers under Extreme Pressures

Han Li, Ying Qin, Byeongkwan Ko, Dipesh B. Trivedi, Debarati Hajra, Mohammed Yasir Sayyad, Lei Liu, Sang-Heon Shim, Houlong Zhuang, and Sefaattin Tongay*

Newly discovered 2D Janus transition metal dichalcogenides layers have gained much attention from a theory perspective owing to their unique atomic structure and exotic materials properties, but little to no experimental data are available on these materials. Here, experimental and theoretical studies establish the vibrational and optical behavior of 2D Janus S–W–Se and S–Mo–Se monolayers under high pressures for the first time. Chemical vapor deposition (CVD)-grown classical transition metal dichalcogenides (TMD) monolayers are first transferred onto van der Waals (vdW) mica substrates and converted to 2D Janus sheets by surface plasma technique, and then integrated into a 500 µm size diamond anvil cell for high-pressure studies. The results show that 2D Janus layers do not undergo phase transition up to 15 GPa, and in this pressure regime, their vibrational modes exhibit a nonmonotonic response to the applied pressures ($d\omega/dP$). Interestingly, these 2D Janus monolayers exhibit unique blueshift in photoluminescence (PL) upon compression, which is in contrast to many other traditional semiconductor materials. Overall theoretical simulations offer in-depth insights and reveal that the overall optical response is a result of competition between the ab-plane (blueshift) and c-axis (redshift) compression. The overall findings shed the very first light on how 2D Janus monolayers respond under extreme pressures and expand the fundamental understanding of these materials.

Theoretically predicted[1] and experimentally demonstrated[2–4] 2D Janus transition metal dichalcogenides (TMDs) are new-class of quantum material with unique atomic structure and material properties. Transition metal atoms in 2D Janus TMDs (Mo or W) are sandwiched between different chalcogen atoms such as sulfur atoms on the top surface and Se atoms at the bottom in S–W–Se as shown in **Figure 1**a,b. This atomic configuration is much different compared to classical TMDs

wherein metal atoms are sandwiched between same chalcogen atoms as well as 2D TMD alloys such as $MoS_{2x}Se_{2(1-x)}$ or $WS_{2x}Se_{2(1-x)}$ wherein different chalcogen atoms are randomly distributed at the top and bottom surfaces.[5–9] Instead, 2D Janus layers are asymmetric along the stacking axis which means they lack out-of-plane mirror symmetry. This unique atomic arrangement leads to a colossal electric field (polarization)[1,2,10] due to uneven cation-anion charge distribution resulting from large electronegativity difference between the top and bottom chalcogens. This can be clearly seen in 2D Janus S-We-Se as shown in Figure 1a. The negative charges cumulate more around sulfur than selenium due to higher electronegativity of sulfur and leads to an electric field built within the 2D Janus unit cell as theoretically demonstrated in the literature.[1,2,10] And the presence of colossal field has indeed been theoretically shown to lead to many exciting properties including giant Rashba splitting,[11] Skyrmion formation,[12,13] rich exciton complexes,[10,14] unique energy conversion routes,[15,16] and others.[2]

Despite these exciting predicted properties and reported fabrication methods, there is few experimental characterization studies[3–4] on 2D Janus TMDs. This includes high-pressure studies which offer a unique way to probe the material behavior when lattice constant is varied by the applied pressure in diamond anvil cell (DAC). While there are a few high-pressure studies on bulk, few-layered, and monolayer thick classical TMDs, the behavior of 2D Janus layers under pressure is not established due to difficulties in sample preparation and integration with the DAC chamber.

In this work, we report on the first high-pressure studies in 2D Janus S–Mo–Se and S–W–Se monolayers from 0 up to 15 GPa. In our studies, we find that the induced colossal field creates added difficulties in transferring 2D Janus layers into only 500 µm culet size DAC. Thus, it was imperative to adopt to two-step fabrication technique inspired by studies on classical TMDs.[4] In this method, classical TMDs are synthesized and transferred onto 2D mica templates using dry-polymer assisted technique,[17] next converted to 2D Janus monolayers, and lastly, 2D Janus/mica heterolayers were transferred into our DAC chamber. In situ Raman and photoluminescence (PL)

H. Li, Y. Qin, D. B. Trivedi, D. Hajra, M. Y. Sayyad, L. Liu, H. Zhuang, S. Tongay
School for Engineering of Matter
Transport and Energy
Arizona State University
Tempe, AZ 85287, USA
E-mail: Sefaattin.tongay@asu.edu
B. Ko, S.-H. Shim
School of Earth and Space Exploration
Arizona State University
Tempe, AZ 85287, USA

The ORCID identification number(s) for the author(s) of this article can be found under https://doi.org/10.1002/adma.202002401.
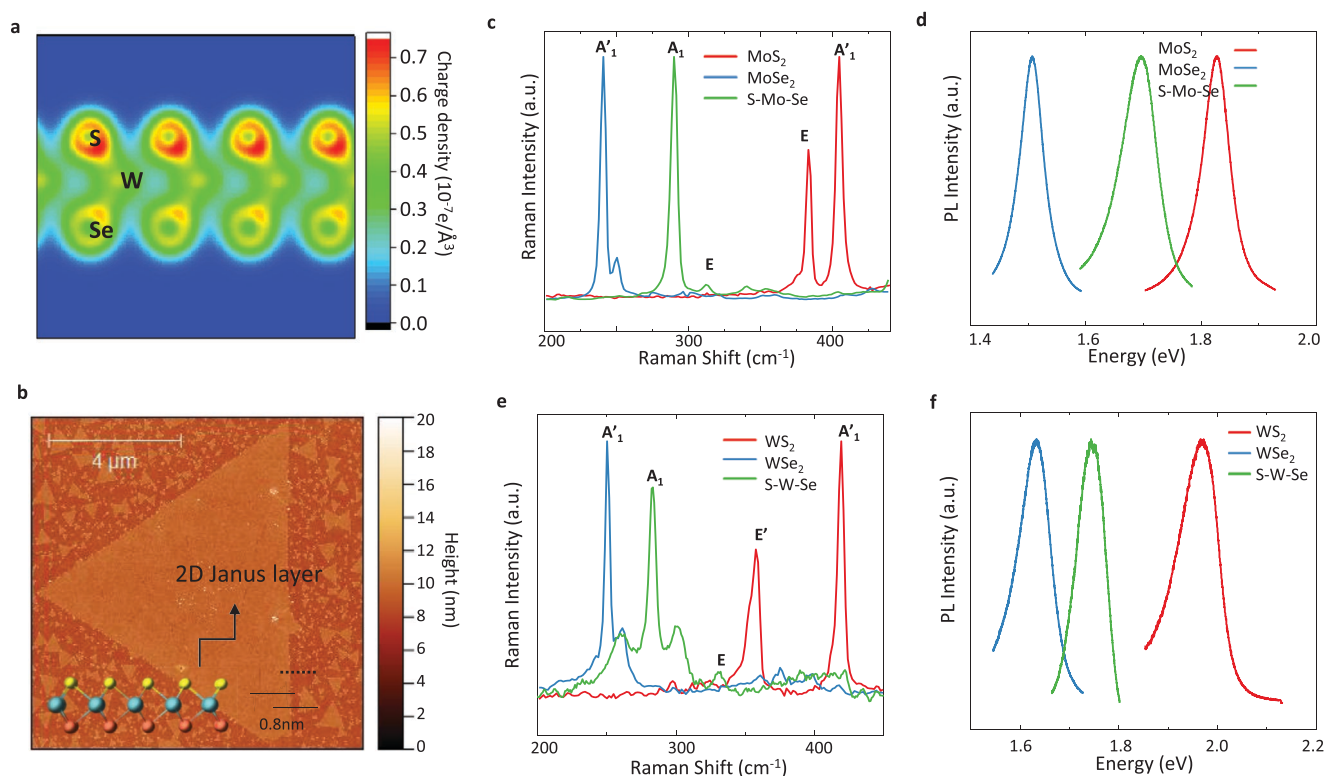
DOI: 10.1002/adma.202002401

Figure 1. a) Calculated charge distribution for 2D Janus TMDs (S–W–Se). b) Atomic force microscopy image of 2D Janus S–W–Se monolayers and AFM line scan given in the inset. c,d) Comparison of Raman and PL spectra for classical MoS_2 and $MoSe_2$ and 2D Janus S–Mo–Se monolayers. e,f) Similar comparisons given for classical WS_2 and WSe2 and 2D Janus S–W–Se monolayers.

spectroscopy techniques were used to investigate their vibrational and optical properties under high pressures. Our experimental and theoretical findings reveal unique excitonic and vibrational responses from 2D Janus layers at high pressures and offer fundamental insights to these material systems.

2D Janus monolayers were synthesized by a two-step technique. In the first step, MoS_2 and WSe_2 monolayers were grown using standard CVD technique and established parameters.[18,19] After classical TMDs are synthesized, we have used home-made inductively coupled RF hydrogen plasma to selectively remove the top selenium/sulfur layer and replace them with sulfur/selenium atoms using sulfur radicals (see method for details) through established growth technique.[4] Atomic force microscopy (AFM) scanning image shows that synthesized 2D Janus S–W–Se (Figure 1b) is rather smooth (RMS < 0.01 nm) and it measures one unit cell (0.7–0.8 nm) in thickness.

The presence of Janus layers has been confirmed by both Raman and photoluminescence spectroscopy techniques. Previous experimental and theoretical studies have already established Raman spectroscopy technique as a fast, nondestructive, and reliable technique to identify 2D Janus layers and distinguish them from 2D classical TMDs as well as their alloys.[2,4,20] The comparison among their Raman is shown in Figure S1 in the Supporting Information. Taking a closer look at Janus S–Mo–Se in Figure 1c shows the most prominent Raman peaks for Janus S–Mo–Se are located at 291 and 350 cm^{-1} which corresponds to A_1 and E modes based on our theoretical vibration studies. We note that these observed Raman peak positions

for S–Mo–Se are completely different from those in 2D MoS_2 (396 and 404 cm^{-1}),[22] 2D $MoSe_2$[23] (241 cm^{-1}) as well as their alloys[24] and allows us to identify Janus formation without any doubt. These results are in full agreement with the published theoretical datasets[10,21] as well as synthesized S–Mo–Se layers.[3,4] Similar arguments can be extended to Raman spectra of Janus S–W–Se: Janus S–W–Se Raman peaks are located at 284 cm^{-1} (A_1 mode) and 330 cm^{-1} (E mode) compared to WSe_2 (240 cm^{-1}), WS_2 (359 and 408 cm^{-1}) (Figure 1e). It is also important to note that FWHM of Janus Raman peaks is as low as 6 cm^{-1}, demonstrating the high crystallinity of Janus monolayers.

In addition to Raman spectra, the measured PL spectra also confirm the formation of Janus monolayers (Figure 1d,f). PL peak position of Janus S–Mo–Se and S–W–Se is located at 1.7 and 1.75 eV which are vastly different from 2D classical TMDs such as MoS_2 (1.86 eV), $MoSe_2$ (1.51 eV), WS_2 (1.97–2.02 eV), and WSe_2 (1.63 eV). PL peak positions for Janus monolayers are fully consistent with the prior theoretical predictions[10,21] and experimentally reported values.[3,4]

Also, scanning transmission electron microscopy (STEM) imaging helped prove the formation of Janus monolayer. In Figure S2 in the Supporting Information, we show a high-angle annular dark-field STEM (HAADF-STEM) image of Janus SWSe converted from WSe_2 in Figure S2a in the Supporting Information, line scans, fast Fourier transform (FFT) and line scan intensity plot in Figure S2b–d in the Supporting Information. Statistical average of the intensity ratio at chalcogen and metal sites is extracted out as 0.366 ± 0.023, while the theoretical intensity
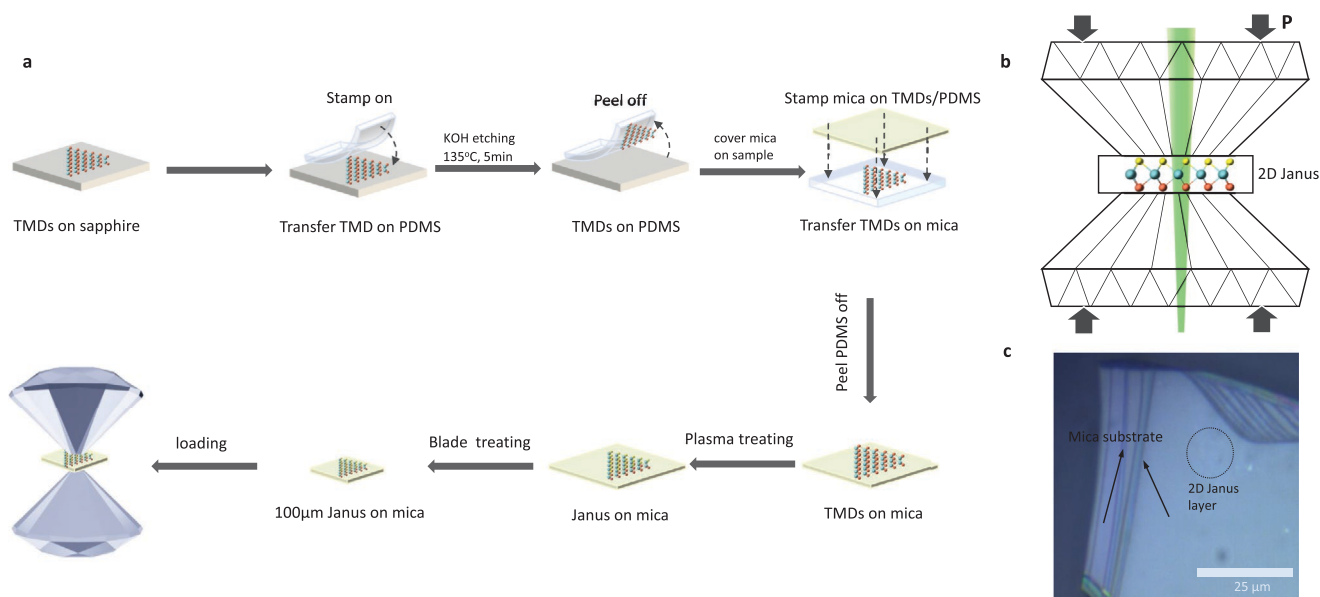
**ADVANCED
SCIENCE NEWS**

www.advancedsciencenews.com

**ADVANCED
MATERIALS**

www.advmat.de

Figure 2. a) The process used for integrating 2D Janus monolayers into DAC chamber. b) Schematic of diamond anvil cell (DAC). c) Optical image of 2D Janus monolayer on mica substrate inside the DAC chamber.

ratio of SWSe (S:Se = 1:1) is 0. 359. Similarly, in Figure S3 in the Supporting Information, STEM collected from Janus SMoSe (converted from MoS_2) is shown and line scan intensity ratio experimentally turned out as 0.898 ± 0.091, while the theoretical intensity ratio of SMoSe (S:Se = 1:1) is 0. 911. Further calculation estimated the conversion rate as 98.2% in SWSe and 98.1% in SMoSe (details in Sections S2–S3 in the Supporting Information). Lastly, we plotted the Raman of our sample with respect to plasma processing time (Figure S4, Supporting Information) from 0 to 18 min. It shows the conversion from the starting material WSe_2 to partial Janus SWSe at 12 and 15 min evidenced by the combination of Janus SWSe Raman peak and WSe_2 Raman peak, and eventually to complete Janus SWSe at 18 min.

To monitor the pressure effects on the material properties, we have used diamond anvil cell (DAC) to apply high pressures to 2D Janus TMDs monolayers. In our early studies, we tried to directly transfer synthesized 2D Janus layers onto diamond cutlets using dry-polymer assisted technique to fabricate samples for high-pressure studies. Our experience shows that unlike classical 2D TMDs layers, 2D Janus layers are much harder to transfer onto the diamond surface presumably due to existing E-field and strong adhesion to the polymer.

Considering these difficulties, we have adopted a direct growth technique (**Figure 2**a). In this method, 2D classical TMDs are first synthesized and transferred onto van der Waals (vdW) mica substrates using a dry polymer assisted method[17] and converted to Janus layers using the technique outlined above. Lastly, the mica substrates are thinned down to around 90 µm in lateral dimensions and 5 µm in thickness. Here, the mica serves as a template (substrate) and offers a solid platform to stabilize 2D Janus layers inside the DAC chamber. Mica substrates (≈90 µm in lateral dimensions) are selected since 2D Janus layers can be transferred onto them by simple stamping technique, owing to mica's chemical inertness, and their vdW layered nature which

allows us to thin them down to few micrometers in thickness. The latter is an important consideration since it is necessary to fit them into limited DAC chamber space. Next, 2D Janus/mica stack was then loaded into the diamond anvil cell with the help of a 10 µm-edge needle. Sodium chloride is used as pressure media which is inert to studied specimens since the material response remains unchanged after full compression and decompression pressure cycle.

Instead of using ruby fluorescence as a pressure gauge, we have used another established[25] diamond Raman peak to measure the pressure. The rationale behind this choice is so that the ruby fluorescence does not screen the 2D Janus PL signal. Prior to our measurements, we have carefully pre-calibrated diamond Raman peaks with respect to pressure using ruby as reference under similar conditions. To prove the effectiveness of our methodology, we applied pressure on monolayer MoS_2 held by mica substrate and collected Raman spectra at different pressure. Figure S5 in the Supporting Information shows that the change in the MoS_2 Raman peak positions with pressure (using our methodology) matches very closely to the data collected by a ruby reference in the literature[25] and shows the efficacy of our approach.

In **Figure 3**a, we show the Raman spectra acquired from 2D Janus S–W–Se at different pressure values. In these Raman data sets, both 2D Janus and mica substrates contribute to the overall spectra wherein the Raman peaks at 265, 405, and 702 cm^{-1} correspond to 1st order Raman modes of mica whereas other two Raman peaks at 284 and 330 cm^{-1} originate from S–W–Se layers as shown in Figure S6 in the Supporting Information.

A closer look at our pressure studies shows that for increasing pressure, these two S–W–Se Raman peaks shifts to higher frequencies as bonds stiffen under extreme pressures. Interestingly, however, the rate at which this stiffening occurs changes dramatically at different pressures. More explicitly, A_1 optical mode (284 cm^{-1}) shown in Figure 3b first stiffens at

ADVANCED
SCIENCE NEWS

www.advancedsciencenews.com

ADVANCED
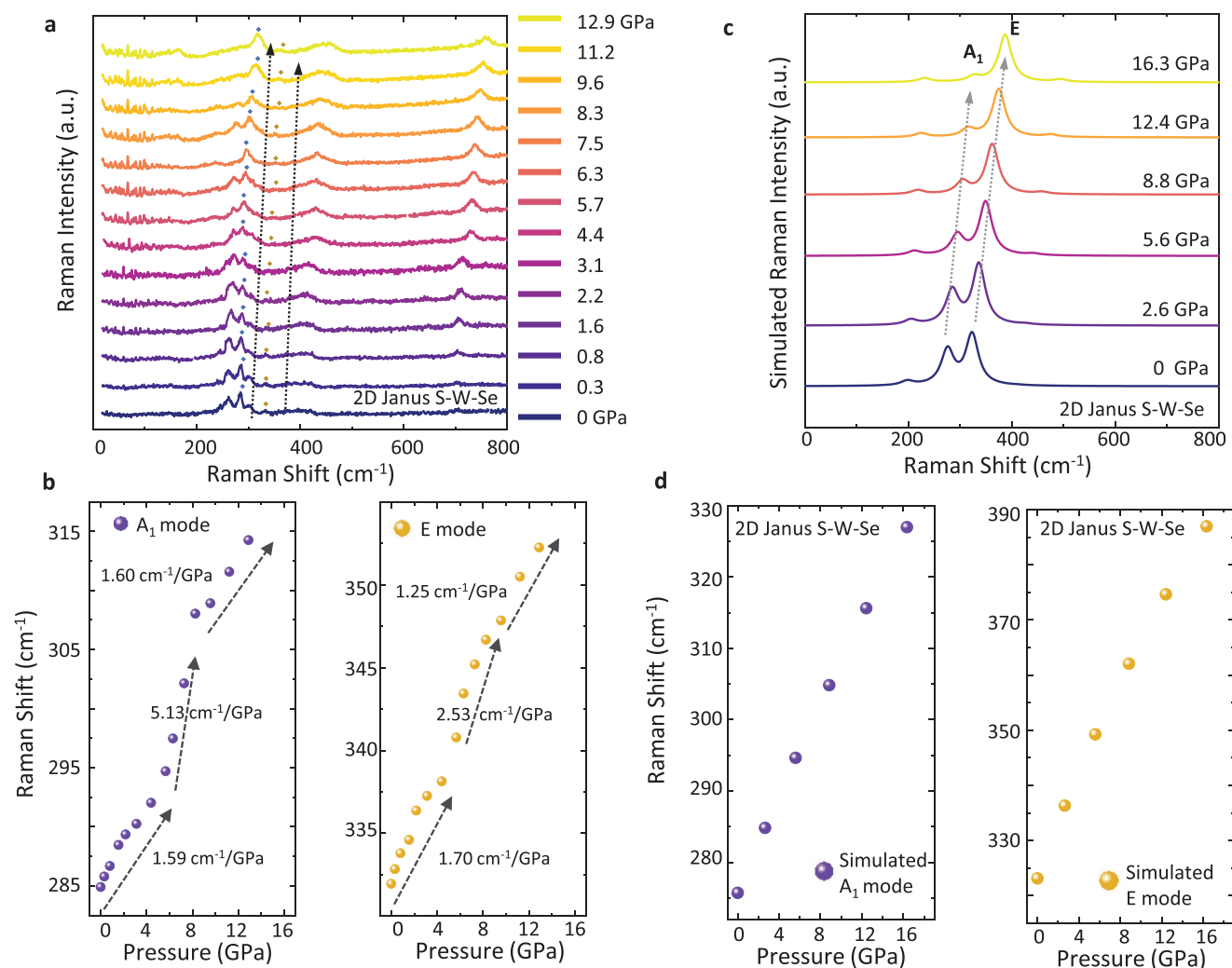**MATERIALS**

www.advmat.de

Figure 3. Vibrational properties of S–W–Se at high pressures. a) Collected Raman spectra for 2D Janus S–W–Se monolayers from low to high pressures. The variation of Raman peak position with pressure. b) A_1 mode at 284 cm^{-1} and E mode at 330 cm^{-1}. c) Theoretically predicted Raman spectra for 2D Janus S–W–Se at different pressures. d) Simulated Raman mode frequencies with pressure for the A_1 and E modes, respectively.

a rate of 1.59 cm^{-1} GPa^{-1} with the estimated Gruneisen parameter of 2.6 from 0 to 4.4 GPa. Further compression from 4.4 to 8.3 GPa, the Raman peak stiffens ≈3 times faster (5.13 cm^{-1} GPa^{-1}) with the Gruneisen parameter of 8.4. At the very high pressures (8.3 to 12.9 GPa), the mode stiffening rate significantly slows down (1.60 cm^{-1} GPa^{-1} and Gruneisen parameter of 2.9) which is much similar to those observed at low-pressure range (0–4.4 GPa). Similar trends were also observed for the E mode at 330 cm^{-1}: from 0 to 3.1 GPa, the stiffening rate is 1.25 cm^{-1} GPa^{-1}; and from 4.4 to 7.5 GPa, the stiffening rate increases to 3.4 cm^{-1} GPa^{-1}; lastly from 8.3 to 12.9 GPa, the stiffening rate is reduced to 1.30 cm^{-1} GPa^{-1}. It is also notable that these trends can be closely reproduced during compression and decompression cycles which means observed results are not an artifact but repeatable across different samples as well as pressure cycles. Even though the rate of stiffening shows sudden changes at critical pressures, this cannot be identified as phase transition since the Raman spectra do not show any significant changes or additional modes with pressure.

These anomalous vibrational effects were also observed in 2D Janus S–Mo–Se monolayers shown in **Figure 4**a–d. 2D Janus S–Mo–Se A_1 and E Raman modes located at 290 and 350 cm^{-1} shifts to higher frequencies for increasing pressures. We note in Figure 4c, during the full cycle of compression and decompression, the Raman shift behavior remains repeatable. Indeed, their behavior shows rather similar effects to those observed in S–W–Se monolayers. Explicitly, the 290 cm^{-1} peak stiffens with a rate of 1.82 cm^{-1} GPa^{-1} from 0 to 4.1 GPa and 1.84 cm^{-1} GPa^{-1} from 8.1 to 12 GPa. In between these two pressure ranges (4.1–7.8 GPa), the Raman peak becomes far more sensitive to the applied pressure and reaches a rate of 2.77 cm^{-1} GPa^{-1}. These $d\omega/dP$ values for 2D Janus layers are rather close to each other in the low (0–4 GPa) and high (8–12 GPa) pressure regimes.

To better understand the vibrational properties of 2D Janus S–W–Se layers at high pressures, we employed density functional theory (DFT) calculations to simulate Raman vibration modes at different compressive strain values and the methodology used is outlined in detail in the experimental section as
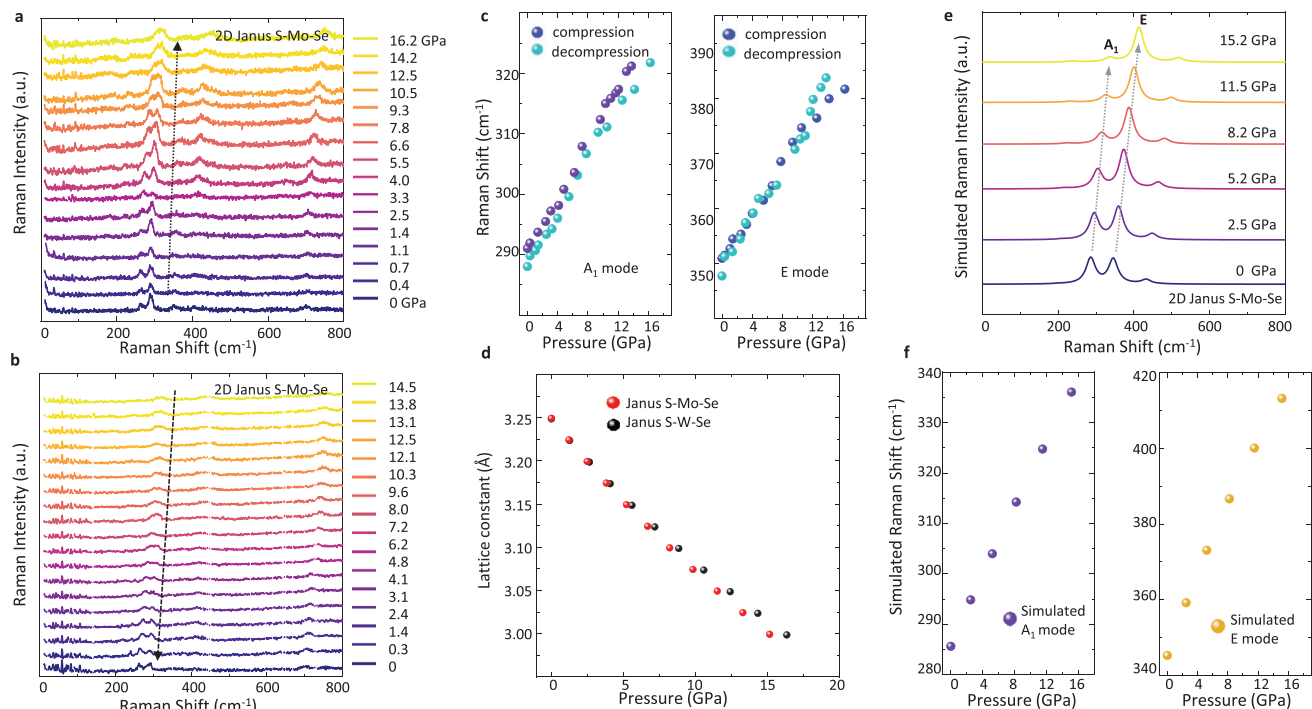
Figure 4. 2D Janus S–Mo–Se under high pressure. a,b) Collected Raman spectra for 2D Janus S–Mo–Se monolayers from low to high pressures during compression (a) and decompression (b). c) Raman peak shift for A_1 and E modes at different pressure values during compression and decompression. d) Theoretically calculated lattice constants at different pressures. e) DFT-simulated Raman spectrum at high pressure. f) Simulated Raman shift of A_1 and E modes versus pressure.

well as supplementary information sections. Figure 3d shows the computed Raman spectra from DFT calculations for 2D Janus S–W–Se monolayers subject to high-pressure deformation. First, we note that both A_1 and E optical modes blueshift with the applied pressure inside the DAC chamber due to increased interatomic interaction strength and effective spring constant. Theoretically, Raman frequencies shift to 316 (A_1) and 375 cm^{-1} (E) at 12.4 GPa which is close to the experimentally observed values at 12 GPa (314 for A_1 and 351 cm^{-1} for the E mode). Similarly, 2D Janus S–Mo–Se yields A_1 and E modes at 336 and 413 cm^{-1} around 15.2 GPa which are still somewhat comparable to the experimental Raman shifts at 321 and 381 cm^{-1}. Experimental pressure trends are similar to theoretically predicted values for 2D Janus S–Mo–Se, though theory produces stronger pressure variation in E mode. We also note that that the different pressure variation rates ($d\omega/dP$) at the low, medium, and high pressure ranges are only experimentally observable and our theoretical simulations did not capture any similar phenomena. The stronger variation in theoretically predicted $d\omega/dP$ as well as absent nonmonotonic $d\omega/dP$ changes with pressure could be attributed to the simplification behind the computational methodology used. More explicitly, 2D Janus layers might be relaxing in a complex form with pressure which is not easy to identify or capture with DFT studies; or second-order Raman effects might be playing a role in the pressure variation of optical modes.

After discussing the vibrational response at high pressure, we shift our focus to excitonic properties of 2D S–W–Se Janus layers under high pressures. We have selected S–W–Se Janus

layers owing to their higher PL intensity compared to Janus S–Mo–Se layers, which allows us to collect clean PL signals when the 2D Janus monolayer is kept in the DAC and NaCl media. For traditional semiconducting materials, compressive pressure is known to reduce the bandgap of the material and if the applied pressure is high enough, it can even cause semiconductor to metal transition. The pressure-induced band reduction effect is generally well explained within the tight-binding approximation as well as more advanced theory simulations.[27–30]

In contrast to these traditional semiconductor materials, 2D Janus layers exhibit rather different pressure dependence as evidenced by the collected PL spectra at different pressures (**Figure 5**a). The overall PL peak position shows very small changes with pressure but has a noticeable amount of blueshift as shown in Figure 5b. From 0 to 3.6 GPa, excitonic peak position increases from 1.78 to 1.84 eV with a rate of 16 meV GPa^{-1}. From 3.9 to 13.6 GPa, the bandgap saturates fast and remains scattered around 1.85 eV. The FWHM of PL spectra also shows a similar trend. From 0 to 3.6 GPa, the FWHM increases from 0.05 to 0.25 eV, and the FWHM remains almost constant between 3.9 and 13.6 GPa. We note that a similar trend can be observed during decompression as shown in Figure S7 in the Supporting Information. As the pressure is reduced from 14.3 to 5.9 GPa, the bandgap fluctuates around 1.84 eV and the bandgap rapidly redshifts from 1.84 to 1.77 eV as the pressure is released from 4 GPa to atmospheric pressure. Since the PL goes back to its original position and FWHM before and after the compression–decompression cycle, and we measure the same PL
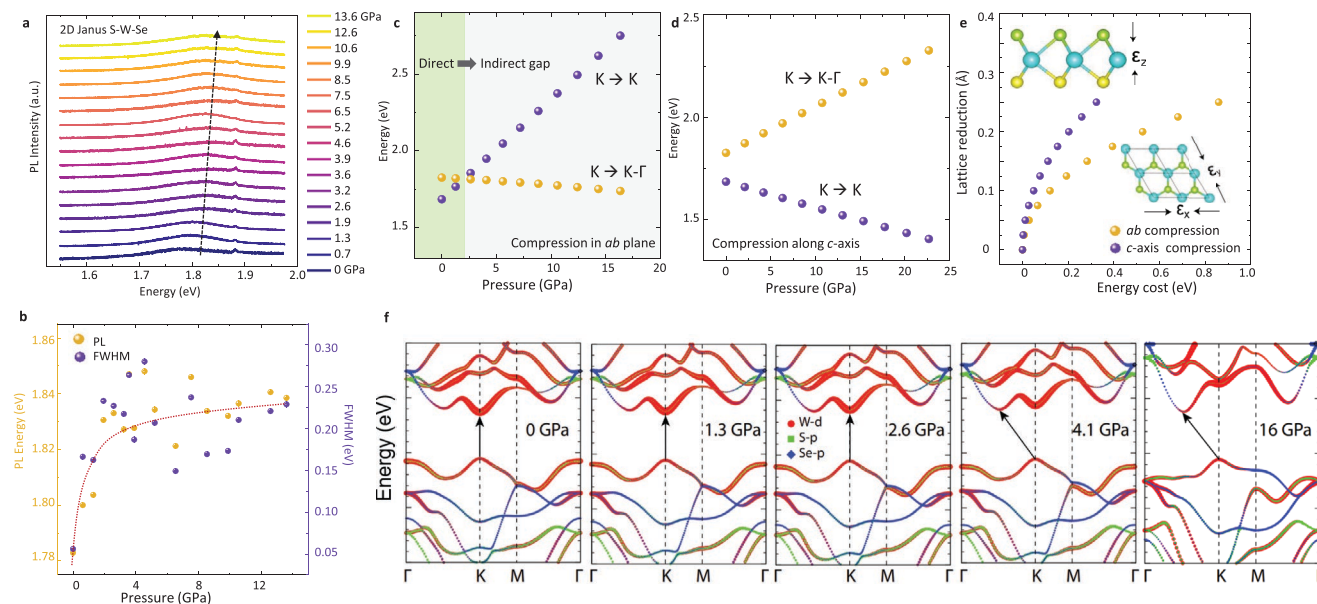
Figure 5. a) Optical properties and band renormalization of SWSe under high pressure. Photoluminescence (PL) spectra collected at different pressures for 2D Janus S–W–Se. b) The variation of PL peak position and FWHM with respect to applied pressure. c,d) Calculated bandgap of 2D Janus S–W–Se under *ab* basal plane (c) and *c* out-of-plane (d) compression. e) Calculated energy cost per single unit cell to reduce lattice constant. f) Calculated orbital-resolved band structures of 2D Janus S–W–Se under *ab* basal plane compression.

peak position trend during cycling, we prove that our sample remains undamaged and the observation is not an artifact. The observed blueshift is clearly different from those observations in traditional semiconductors as well as vdW TMDs crystals.[29–31] It is also noteworthy that the change in the bandgap is rather small (16 meV GPa^{-1}) compared to other traditional systems (20–50 meV GPa^{-1}).[32] Interestingly, however, our results show that the observed blueshift at high pressures has a close resemblance to those observed for 2D TMDs monolayers[26,33–35] which will be discussed in detail later.

What is the origin of this anomalous pressure dependence? In principle, one can offer fundamental insights to this blueshift trend under pressure through comprehensive DFT calculations. But the pressure applied to 2D Janus layers in DAC chamber can be rather complex considering the atomically thin nature of the material itself. To simplify the problem, we have deconvoluted the pressure acting on 2D Janus layers into two parts, namely compression strictly in the *ab*-plane and along the *c*-axis. This enables us to understand the bandgap change coming directly from these two types of compression. In the past, this theoretical simplification was successfully applied to classical TMDs[36,37] and in this work extended to 2D Janus layers. Here, the *c*-axis compression for 2D Janus monolayer refers to the reduction in the unit cell (S to Se distance) as opposed to the reduction in interlayer distance since the vdW gap is absent in the monolayer limit.

Our results show that that *ab* plane compression leads to an increase of direct bandgap (K–K) as shown in purple in Figure 5c. Meanwhile, the indirect bandgap (K to K–Γ) decreases monotonically (orange in Figure 5c). The competition between these two transitions ultimately induces direct to indirect gap transition in 2D Janus S–W–Se monolayers. Previously, direct

to indirect bandgap transition was observed in classical TMD monolayers.[26,34] Figure 5f displays the orbital-resolved band structures of 2D Janus S–W–Se under different *ab* compressive strains. As pressure increases up to 1.3 GPa, the valence band maximum (VBM) remains at the K point, while the conduction band minimum (CBM) moves apart from the VBM owing to the weakened hybridizations between tungsten *d* and chacolgen (S, Se) *p* orbitals. For higher pressure, the energy levels (between the Γ and K points) that are originally comparable to the CBM start to be significantly affected by pressure. In particular, the lowest energy of these energy levels becomes a new CBM at the pressure of about 2.6 GPa and above the semiconductor undergoes direct to indirect transition. More importantly, if only *ab* plane compression is taken into account, the bandgap initially blueshifts and remains nearly unchanged at higher pressures like our experimental observations. At the same time, compression along the *c*-axis (unit cell thickness reduction) causes direct bandgap value to decrease linearly with pressure (Figure 5d purple), while the indirect bandgap increases (Figure 5d orange). Different from *ab* compression, direct bandgap values are always smaller than indirect bandgap values, which suggests that the bandgap remains direct under all pressures.

At first sight, this finding suggests that the *ab* compressive strain must be dominating the deformation mechanism over *c*-axis which in turn leads to the overall PL peak shifting to slightly higher energies. While this might be sufficient to gain a fundamental insight, we caution that the competition between *ab* and *c* compression should be ultimately dictated by the energy cost per unit cell (Figure 5e) to induce the same amount of distance reduction in the *ab* and *c* directions. Our results show that the energy costs of small strains along the *ab* and *c* directions are nearly the same but it becomes more energy-consuming for

**ADVANCED
SCIENCE NEWS**
www.advancedsciencenews.com

**ADVANCED
MATERIALS**
www.advmat.de

the larger compressive strains in *ab* basal plane. Considering this, we argue that other factors in the experimental set up such as the presence of the substrate (which is absent in our simulations) might be causing such difference. For example, the pressure exerted during our measurements might be transferred to reducing the vdW gap between the mica substrate and 2D Janus layer as opposed to *c*-axis unit cell reduction as assumed in our theory calculations. This would imply that the external energy is successfully transferred to *ab* plane deformation but the vertical pressure is mostly distributed to reducing the vdW gap at the substrate/2D layer interface. In this view, our experimental observations and theoretical simulations can be explained phenomenologically, though future more comprehensive studies are needed to gain further insights into how pressure is distributed in the 2D Janus layers.

In summary, our work has experimentally and theoretically established the vibrational and optical properties of 2D Janus S–W–Se and S–Mo–Se monolayers under high pressures for the first time. 2D Janus layers exhibit a blueshift in PL under high pressure and have an unusually small response to applied pressure which is much different compared to many other traditional semiconductors. Our results also mark the first studies on the vibrational behavior of 2D Janus monolayers under extreme pressures. These studies reveal that 2D Janus layers do not undergo phase transition up to 15 GPa while establishing the vibrational response of 2D Janus layers under extreme pressures. Comprehensive ab initio simulations offer insights into optical and vibrational response and reveal that the overall optical response is a result of competition between the *ab*-plane (blueshift) and *c*-axis (redshift) compression while correlating vibrational responses to theoretical simulations. The combined experimental results and theoretical insights not only shed the first light on how 2D Janus layers respond to extreme pressures but also expand our understanding of these unique 2D Janus materials.

Experimental Section

Chemical Vapor Deposition of WSe₂ and MoS₂: WSe₂ monolayers are grown with chemical vapor deposition (CVD) in single-zone Lindberg tube furnace. 60 mg WO₃ was placed in alumina boat located in the center of 1-inch tubing and 1.5 g Se was placed 18 cm upstream in an alumina crucible. Double side polished sapphire substrates are placed directly on top of WO₃ precursor. 80 sccm carrier gas (Ar: H₂ = 9: 1) was used to flush the system before heating for 15 min to eliminate air. The furnace was heated up to 850 °C in 17 min and kept at 850 °C for 20 min before natural cooling. MoS₂ monolayers were grown in the same setup with MoO₃ and S as precursors. 3 mg MoO₃ was placed in alumina boat with 285 nm SiO₂/Si substrate on top. Se was placed 18 cm upstream in an alumina crucible. 20 sccm N₂ was used as the carrier gas. The furnace was heated up to 680 °C in 18 min and kept at 680 °C for 10 min before natural cooling.

TMDs Transfer onto Mica Templates: WSe₂ and MoS₂ monolayers were transferred onto mica using a polymer-assisted transfer method. A thin film of poly(dimethylsiloxane) (PDMS) was placed on as-grown WSe₂/MoS₂. Then monolayer on PDMS thin film was obtained by etching in 2 mol L⁻¹ KOH solvent at 135 °C for 5 min. Dried PDMS thin film was pressed on mica substrate and then slowly peeled off which allows transferring of Janus monolayers onto mica substrate.

Conversion of TMDs to Janus Structure: In a 1-inch quartz tube, base pressure of 15 mTorr was reached with a mechanical pump followed by a flowing of 20 sccm H₂ to keep system pressure at 250 mTorr. Inductively

coupled H₂ plasma was ignited with 15 W RF power source. After marking the visible plasma tail position, TMDC on mica was placed 2 cm upstream of plasma tail and source chalcogen (Se for MoS₂ conversion and S for WSe₂ conversion) powder was placed 9 cm upstream of plasma tail. The same evacuation procedure was done before plasma ignition, and 10 and 18 min processing time were used for sulfurization and selenization process respectively.

Janus Transfer into Diamond Anvil Cell (DAC) and In Situ Photoluminescence and Raman Spectroscopy: Converted Janus on mica was cut with blade and transferred into DAC using 10 μm-edge needle under microscope. Janus monolayer together with supporting mica substrate were loaded into the gasket hole with 210 μm diameter and 50 μm thickness. NaCl was used as pressure media to transmit pressure on sample. The diamond Raman peak was used as pressure gauge to figure out in situ pressure in the DAC. PL and Raman spectra were measured in situ by the homemade spectroscopy with 532 nm green laser in a backscattering configuration, and the grating was 1200 mm⁻¹. The laser spot size was ≈4 μm. Data was collected with power at the sample of 6 mW for Raman and 1.3 mW for PL measurements.

Atomic Force Microscopy (AFM): NT-MDT modular AFM was used for AFM measurement. The sample height profile was recorded by noncontact mode and the images were plotted with Gwyddion software.

Density Function Theory (DFT) Calculations: DFT calculations were performed using the Vienna Ab initio Simulation Package (VASP).[38,39] The PBE functional was used for describing the electron exchange-correlation interactions.[40] The projector-augmented wave (PAW) potentials and a cut-off energy of 600 eV were also used for the plane waves and a Γ-centered $15 \times 15 \times 1$ *k*-point grid for the monolayer structures and a $8 \times 8 \times 6$ *k*-point grid for the bulk structures. Dipole corrections were included in the DFT calculations. All the monolayer structures were simulated via surface slab models with a vacuum spacing of 18 Å. Note that one limitation of the DFT calculations was that an isolated Janus monolayer sheet was being modeled in vacuum, so the environmental effects from, e.g., the substrate was not considered. In obtaining the thickness of bulk SWSe and SMoSe, the DFT-D3 method was adopted to approximate the interlayer van der Waals forces.[41] Note that we performed spin–orbital (SOC) calculations and found that the SO splitting energies at valence band maximum (at the K point) of monolayer SMoSe and SWSe were 0.17 and 0.44 eV, respectively. While SOC was important, valley effects were not studied in this work due to complexities in DAC geometry and detection and thus use of PBE did not impact the conclusions. To obtain the pressure-free ground state structures, the in-plane lattice constants and atomic coordinates of the monolayer structures and all lattice constants and atomic coordinates of the bulk structures were fully optimized to meet the force threshold of 0.01 eV Å⁻¹. The Raman spectra were computed using the Poezag and Pederson method.[42] For the compressions in the ab plane or along the c direction, the pressure was estimated using the equation $P = \Delta E / \Delta V$, where ΔE is the energy increase and ΔV is the volume decrease with reference to the zero-pressure structure. ΔE was obtained by subtracting the ground state energy from the energy of Janus monolayer under strain. The volume of the monolayer lattice was hS. h was the thickness of the lattice, which was estimated by the interlayer distance in bulk SW(Mo)Se as shown in Supplementary Figure S8 in the Supporting Information. S wass the area of the lattice in ab plane. For the ab compression, it was assumed that the thicknesses of the Janus structures were fixed, so ΔV is equal to $h\Delta S$, where ΔS was the change of area in ab plane and can be obtained by the strain value; for the c compression, it was assumed that the in-plane lattice constant was fixed, so ΔV equals to $\Delta h \cdot S$, where Δh was the change of the thickness and can be obtained by the strain in c direction.

STEM sample transfer and characterization: CVD grown Janus monolayers were transferred onto the Quantifoil TEM grid by polymer assisted transfer method. First, the copper grid was kept on the substrate with carbon-side down and covered with poly(methyl methacrylate) (PMMA). Then, the substrate was dried at 120 °C for 2 min followed by etching with KOH at 70 °C to separate the substrate and the sample. After the separation, PMMA was removed by immersing the grid in acetone for few minutes. Finally, any residual impurities were removed by washing the grid with deionized water and dried in ambient.

High-angle annular dark-field images (HAADF) of monolayer Janus materials were acquired in a Nion UltraSTEM 200 scanning transmission electron microscope with third and fifth order aberration correctors and a cold field-emission electron source. For image acquisition an area of the sample on a carbon-hole was selected for each case. The microscope was operated at an accelerating voltage of 60 keV to minimize specimen damage by electron beam radiation. A probe current of ≈100 pA and convergence semi-angle of ≈30 mrad was selected as imaging conditions. EDX mapping of elemental composition was carried out by the same microscope under same conditions. Recorded STEM images were noise-filtered to get a clearer atomic intensity using the Digital Micrograph software. The diffractograms were obtained by performing Fourier transforms of the images which verifies hexagonal projection symmetry of the monolayers. All line-scans on these images were measured along the armchair directions as shown in the figures.

Supporting Information

Supporting Information is available from the Wiley Online Library or from the author.

Conflict of Interest

The authors declare no conflict of interest.

Keywords

[1] Y. C. Cheng, Z. Y. Zhu, M. Tahir, U. Schwingenschlögl, *Europhys. Lett.* **2013**, *102*, 57001.

[2] Y. Q. Mehmet yagmurcukardes, S. Ozen, M. Sayyad, F. M. Peeters, S. Tongay, H. Sahin, *Appl. Phys. Rev.* **2020**, *7*, 011311.

[3] A.-Y. Lu, H. Zhu, J. Xiao, C.-P. Chuu, Y. Han, M.-H. Chiu, C.-C. Cheng, C.-W. Yang, K.-H. Wei, Y. Yang, Y. Wang, D. Sokaras, D. Nordlund, P. Yang, D. A. Muller, M.-Y. Chou, X. Zhang, L.-J. Li, *Nat. Nanotechnol.* **2017**, *12*, 744.

[4] J. Zhang, S. Jia, I. Kholmanov, L. Dong, D. Er, W. Chen, H. Guo, Z. Jin, V. B. Shenoy, L. Shi, J. Lou, *ACS Nano* **2017**, *11*, 8192.

[5] J. Lin, J. Zhou, S. Zuluaga, Y. Peng, M. Gu, Z. Liu, S. T. Pantelides, K. Suenaga, *ACS Nano* **2018**, *12*, 894.

[6] G. Wang, C. Robert, A. Suslu, B. Chen, S. Yang, S. Alamdari, I. C. Gerber, T. Amand, X. Marie, S. Tongay, B. Urbaszek, *Nat. Commun.* **2015**, *6*, 10110.

[7] B. Huang, M. Yoon, B. G. Sumpter, S.-H. Wei, F. Liu, *Phys. Rev. Lett.* **2015**, *115*, 126806.

[8] S. Tongay, D. S. Narang, J. Kang, W. Fan, C. H. Ko, A. V. Luce, K. X. Wang, J. Suh, K. D. Patel, V. M. Pathak, J. B. Li, J. Q. Wu, *Appl. Phys. Lett.* **2014**, *104*, 012101.

[9] J. Kang, S. Tongay, J. B. Li, J. Q. Wu, *J. Appl. Phys.* **2013**, *113*, 143703.

[10] F. Li, W. Wei, H. Wang, B. Huang, Y. Dai, T. Jacob, *J. Phys. Chem. Lett.* **2019**, *10*, 559.

[11] K. Ishizaka, M. S. Bahramy, H. Murakawa, M. Sakano, T. Shimojima, T. Sonobe, K. Koizumi, S. Shin, H. Miyahara, A. Kimura, K. Miyamoto, T. Okuda, H. Namatame, M. Taniguchi, R. Arita, N. Nagaosa, K. Kobayashi, Y. Murakami, R. Kumai, Y. Kaneko, Y. Onose, Y. Tokura, *Nat. Mater.* **2011**, *10*, 521.

[12] J. Yuan, Y. Yang, Y. Cai, Y. Wu, Y. Chen, X. Yan, L. Shen, *Phys. Rev. B* **2020**, *101*, 094420.

[13] J. Liang, W. Wang, H. Du, A. Hallal, K. Garcia, M. Chshiev, A. Fert, H. Yang, *Phys. Rev. B* **2020**, *101*, 184401.

[14] F. Li, W. Wei, P. Zhao, B. Huang, Y. Dai, *J. Phys. Chem. Lett.* **2017**, *8*, 5959.

[15] D. Er, H. Ye, N. C. Frey, H. Kumar, J. Lou, V. B. Shenoy, *Nano Lett.* **2018**, *18*, 3943.

[16] A. C. Riis-Jensen, M. Pandey, K. S. Thygesen, *J. Phys. Chem. C* **2018**, *122*, 24520.

[17] C.-G. Andres, B. Michele, M. Rianda, S. Vibhor, J. Laurens, S. J. v. d. Z. Herre, A. S. Gary, *2D Mater.* **2014**, *1*, 011002.

[18] B. Liu, M. Fathi, L. Chen, A. Abbas, Y. Ma, C. Zhou, *ACS Nano* **2015**, *9*, 6119.

[19] K. Liu, Q. Yan, M. Chen, W. Fan, Y. Sun, J. Suh, D. Fu, S. Lee, J. Zhou, S. Tongay, J. Ji, J. B. Neaton, J. Wu, *Nano Lett.* **2014**, *14*, 5097.

[20] R. Li, Y. Cheng, W. Huang, *Small* **2018**, *14*, 1802091.

[21] A. Kandemir, H. Sahin, *Phys. Chem. Chem. Phys.* **2018**, *20*, 17380.

[22] C. Lee, H. Yan, L. E. Brus, T. F. Heinz, J. Hone, S. Ryu, *ACS Nano* **2010**, *4*, 2695.

[23] S. Tongay, J. Zhou, C. Ataca, K. Lo, T. S. Matthews, J. B. Li, J. C. Grossman, J. Q. Wu, *Nano Lett.* **2012**, *12*, 5576.

[24] Q. Feng, N. Mao, J. Wu, H. Xu, C. Wang, J. Zhang, L. Xie, *ACS Nano* **2015**, *9*, 7450.

[25] Y. Akahama, H. Kawamura, *J. Appl. Phys.* **2006**, *100*, 043516.

[26] A. P. Nayak, T. Pandey, D. Voiry, J. Liu, S. T. Moran, A. Sharma, C. Tan, C.-H. Chen, L.-J. Li, M. Chhowalla, *Nano Lett.* **2015**, *15*, 346.

[27] H. Li, Y. Qin, B. Shan, Y. Shen, F. Ersan, E. Soignard, C. Ataca, S. Tongay, *Adv. Mater.* **2020**, *32*, 1907364.

[28] X. Ren, X. Yan, A. S. Ahmad, H. Cheng, Y. Li, Y. Zhao, L. Wang, S. Wang, *J. Phys. Chem. C* **2019**, *123*, 15204.

[29] F. Dybała, M. P. Polak, J. Kopaczek, P. Scharoch, K. Wu, S. Tongay, R. Kudrawiec, *Sci. Rep.* **2016**, *6*, 26663.

[30] J. Kopaczek, M. P. Polak, P. Scharoch, K. Wu, B. Chen, S. Tongay, R. Kudrawiec, *J. Appl. Phys.* **2016**, *119*, 235705.

[31] R. Oliva, M. Laurien, F. Dybala, J. Kopaczek, Y. Qin, S. Tongay, O. Rubel, R. Kudrawiec, *npj 2D Mater. Appl.* **2019**, *3*, 20.

[32] S.-H. Wei, A. Zunger, *Phys. Rev. B* **1999**, *60*, 5404.

[33] L. Fu, Y. Wan, N. Tang, Y.-m. Ding, J. Gao, J. Yu, H. Guan, K. Zhang, W. Wang, C. Zhang, *Sci. Adv.* **2017**, *3*, 1700162.

[34] X. Fu, F. Li, J.-F. Lin, Y. Gong, X. Huang, Y. Huang, H. Gao, Q. Zhou, T. Cui, *J. Phys. Chem. C* **2018**, *122*, 5820.

[35] X. Fu, F. Li, J.-F. Lin, Y. Gong, X. Huang, Y. Huang, B. Han, Q. Zhou, T. Cui, *J. Phys. Chem. Lett.* **2017**, *8*, 3556.

[36] A. P. Nayak, S. Bhattacharyya, J. Zhu, J. Liu, X. Wu, T. Pandey, C. Jin, A. K. Singh, D. Akinwande, J.-F. Lin, *Nat. Commun.* **2014**, *5*, 3731.

[37] S. Tongay, H. Sahin, C. Ko, A. Luce, W. Fan, K. Liu, J. Zhou, Y. S. Huang, C. H. Ho, J. Yan, D. F. Ogletree, S. Aloni, J. Ji, S. Li, J. Li, F. M. Peeters, J. Wu, *Nat. Commun.* **2014**, *5*, 3252.

[38] G. Kresse, J. Furthmüller, *Phys. Rev. B* **1996**, *54*, 11169.

[39] G. Kresse, J. Hafner, *Phys. Rev. B* **1993**, *47*, 558.

[40] J. P. Perdew, K. Burke, M. Ernzerhof, *Phys. Rev. Lett.* **1996**, *77*, 3865.

[41] S. Grimme, J. Antony, S. Ehrlich, H. Krieg, *J. Chem. Phys.* **2010**, *132*, 154104.

[42] D. Porezag, M. R. Pederson, *Phys. Rev. B* **1996**, *54*, 7830.